Inert Trace Constituent Transport in Sigma and Hybrid Isentropic–Sigma Models. Part II: Twelve Semi-Lagrangian Algorithms

FRED M. REAMES* AND TOM H. ZAPOTOCNY

Space Science and Engineering Center, University of Wisconsin—Madison, Madison, Wisconsin

(Manuscript received 6 August 1997, in final form 23 February 1998)

ABSTRACT

Part I of this paper examined nine trace constituent advection algorithms as applied in channel versions of the University of Wisconsin hybrid isentropic–sigma (θ–σ) and sigma (σ) models. This paper examines the performance of 12 semi-Lagrangian transport (SLT) algorithms in the same models. The interpolants of trace constituent include second- through twelfth-order Lagrangian, an overlapping polynomial, a quasi-monotonic scheme, and two sixth-order schemes that employ derivative estimates. Additional experiments are performed that emulate the SLT algorithm in the NCAR Community Climate Model 2. As in Part I, these three-dimensional simulations are under adiabatic conditions so that conservation of the initial trace constituent maximum on an isentropic surface, and conservation of the areas between any two constituent contours, can be used as objective measures of SLT algorithm accuracy. Further, the experiments provide comparisons not only between the different SLT formulations but also between their performance in models using θ and σ coordinates.

Similar to Part I, an important result of the experiments is that comparison of algorithms is most revealing under three-dimensional transport within a baroclinic wave in which vertical transport is important. The experiments also show 1) that the ''cascade'' interpolation scheme is a reasonable method of greatly reducing computation time in SLT without affecting accuracy; 2) that ''shape-preserving'' interpolation schemes reduce accuracy in both the θ–σ and σ models; and 3) that Lagrangian interpolants of tenth and twelfth order do not significantly improve results. Comparisons to results in Part I suggest that the conservation of second-order moments advection scheme is the most consistent of all options tested.

1. Introduction

After the Global Weather Experiment, research in numerical weather prediction (NWP) steadily advanced the skill of forecasting the large-scale circulation patterns of most meteorologically significant fields, such as pressure, temperature, and winds (Kalnay et al. 1990), but the skill in predicting precipitation did not improve as rapidly (Junker and Hoke 1990). In response to this problem, Williamson (1990) suggested that semi-Lagrangian transport (SLT) techniques should be used to replace spectral methodologies for the transport of water vapor and other trace constituents. Recently, many additional publications have examined various SLT techniques, and following Williamson's suggestion (1990), SLT has been utilized for water vapor and trace constituents within the National Center for Atmospheric Research Community Climate Model (CCM2) and other models.

This study investigates and compares numerous SLT algorithms in a fashion similar to that of Reames and Zapotocny (1999; hereafter Part I), who studied advection algorithms. Transport is examined within a synoptic-scale wave undergoing baroclinic amplification, thus including, unlike most comparisons of transport algorithms, the third dimension of vertical transport. The tests were conducted with channel versions of the University of Wisconsin (UW) hybrid isentropic–sigma (θ–σ) model and a nominally identical sigma (σ) model. As shown in Part I, the 48-h predictions of standard synoptic fields by two vertical resolutions of the θ–σ model and four resolutions of the σ model are extremely similar.

Under the adiabatic conditions of this experiment, both the maximum value of an inert trace constituent and the area between any two trace constituent contour values on an isentropic surface, implicit or explicit, should remain constant throughout integration. Comparisons of these features on an isentropic level at 48 h to corresponding values in the initial distribution therefore provide objective measures of transport accuracy. With these means of comparison, the tests com-

* Current affiliation: Department of Mechanical Engineering, University of Wisconsin—Madison, Madison, Wisconsin

Corresponding author address: Dr. Fred M. Reames, SSEC, University of Wisconsin—Madison, 1225 West Dayton Street, Madison, WI 53706-1695.

pare SLT algorithms, the effects of model vertical resolution, and the use of θ coordinates in models compared to the more conventional σ coordinate.

Section 2 briefly describes the models and the specifics of the various SLT algorithms. Results of the 48-h trace constituent maxima are reviewed in section 3 and a discussion concludes in section 4.

2. The models, trace constituents, and semi-Lagrangian algorithms

a. The models and initial trace constituent distributions

Both the θ–σ and σ models are described in Part I, with greater detail on the θ–σ model in Pierce et al. (1991) and on the σ model in Johnson et al. (1993). Both models are hydrostatic and exclude orography. They are gridpoint models with 1.5° spacing in a domain extending 45° zonally, with cyclic boundary conditions, and meridionally from 10° to 70°. The models use second-order finite differencing (Kurihara and Holloway 1967) for the advection of mass, momentum, and energy, and a 3-min Matsuno (1966) time step. As in Part I, the integrations are limited to 48 h.

Two θ–σ models were used, denoted as θ–σ(5) and θ–σ(3.33), where the number in parentheses represents model-layer thickness (K) in the θ domain. Both these models have three equally spaced layers of total 100 mb in the σ domain, which represent the planetary boundary layer (PBL). Mass, momentum, and energy are advected across the interface between the θ and σ domains but not trace constituent, in the experiments here; this restriction occurs because the experiments are under adiabatic conditions and attention is restricted to constituent transport in the 310 K isentropic layer, which does not intersect the σ domain at any time during the 48-h integrations. This greatly simplifies implementation of the various SLT algorithms because vertical interpolations across the domain interface are not necessary.

Four σ models were used: the σ(19), σ(27), σ(35), and σ(43), where the number shows the total vertical layers. Each σ model has three equally spaced layers as similar as possible to the σ-coordinate PBL of the θ–σ models; the remaining 16, 24, 32, or 40 layers, respectively, are equally spaced to the model top at 50 mb. By comparison, the θ–σ(5) model has the lowest resolution of the six models, with an average of approximately 13 layers, and the σ(43) has approximately twice the number of vertical layers as the θ–σ(3.33), which averages 19 layers. (The number of layers in the θ–σ models is not an integer since it depends on local thermal structure, which is a function of latitude, longitude, and time.)

Two analytically specified trace constituent distributions, shown in Fig. 2 of Part I, are inserted into the initial atmospheres. Of these, the ''310K'' distribution has maximum trace constituent located vertically on the 310 K isentropic level, with exponential decreases as a function of θ above and below. The ''660P'' distribution is centered vertically at a constant pressure of approximately 660 mb, with exponential decreases vertically as a function of pressure. Both distributions decrease exponentially with horizontal distance from their center point, which is at the middle of the domain longitudinally and slightly south of the channel's center latitudinally where the isentropic surfaces are steeply sloped. Interpolations from σ to θ coordinates, when required, are computed as linear with respect to p^{κ}, where $\kappa = R_d/c_p$.

b. Semi-Lagrangian transport of inert trace constituent

In these experiments, the application of SLT is only to inert trace constituent and not to mass, momentum, or energy. In the same fashion as CCM2, the winds causing SLT are determined by the underlying model. Under these conditions, trace constituent q evolves as

$$q(\mathbf{x}, t + \Delta t) = q(\mathbf{x} - \mathbf{d}, t), \tag{1}$$

where $\mathbf{x}$ is three-dimensional position and $\mathbf{d}$ is the displacement vector describing the position changes of the parcel during the time interval Δt. As in most SLT applications, the positions $\mathbf{x}$ are at the grid points, the ''arrival points,'' and the positions $\mathbf{x} - \mathbf{d}$ are the ''departure points.'' Equation (1) raises three questions: the method of computing the displacement vectors $\mathbf{d}$, the size of Δt, and the computation—that is, interpolation—of $q(\mathbf{x} - \mathbf{d}, t)$ from the values of $q(\mathbf{x}, t)$.

1) THE DISPLACEMENT VECTORS

In all cases, the displacement vectors were computed from the velocities in a semi-implicit fashion. For a single model time step Δt, ''trial'' departure points were computed using the wind velocities at the model grid points, that is, $\mathbf{d} = \mathbf{x} - \mathbf{u}'\Delta t$; the midpoints of these trial positions were determined; velocities $\mathbf{u}'$ were interpolated from the grid points to these midpoints; and the final arrival points were $\mathbf{d}' = \mathbf{x} - \mathbf{u}'\Delta t$. When $\Delta t = 5$ or 15 time steps, two different procedures were used. In the first, hereafter the ''one step,'' the velocity vectors were computed as averages of the velocities before and after the time interval. The second, hereafter ''multiple step,'' computed the displacement vectors as the sum of one-step displacement vectors using the velocities saved for each grid point at each model time step. Each partial displacement vector was computed in the same semi-implicit fashion as the one step: a trial vector was computed using velocities interpolated to the ''partial arrival point'' and the final vector was then computed with velocities interpolated to the center of the trial vector. In principle, the multiple-step displacement vectors, which utilize all available velocity data,

should be more accurate than the one step, which use data only at the beginning and end of the time interval.

As noted, the displacements **d** depend on interpolation of velocities. In all cases other than the CCM2 emulations, velocities were interpolated linearly from the nearest grid points. In the θ–σ model, these interpolations were all two-dimensional since the simulations were under adiabatic conditions, that is, $\dot{\theta} = 0$. In the σ model, the three-dimensional linear interpolations used velocities from the eight nearest grid points.

In the experiments emulating CCM2, the velocities were computed with the Lagrangian cubic, or fourth order, interpolation [also one of the interpolants used for $q(\mathbf{x} - \mathbf{d}, t)$, described in section 2b(2)]. The first guess values for the CCM2 velocities were computed at the midpoints of the displacement vectors for the preceding time interval, rather than at the arrival points. Only the one-step displacement vector computations were used for the CCM2 experiments, with the velocities averaged over all time steps of the time intervals. For example, six velocities were averaged for the five–time step time interval experiments: the velocities before the time interval and at the end of each of the five time steps.

2) The size of the time steps

The typical procedure in applying (1) is to use the three-dimensional wind velocities to determine the **d**'s, and then to interpolate the $q(\mathbf{x} - \mathbf{d}, t)$ from the known $q(\mathbf{x}, t)$. To use Δt larger than one time step, the velocities must be saved as the model is integrated forward, so that the **d**'s may be computed as backward trajectories. In principle, the SLT time step in this process can be as large as desired, but logical requirements and computer limitations can produce practical limits. To illustrate these points, consider SLT in a one-dimensional grid in which the points are located at x_i, and the velocities, denoted as u_i, are positive. Consider now the computations for an arbitrary grid point: arrival position x_3. In the first step of the semi-implicit computation, described in section 2b.1, the trial departure point would be $x_3 - u_3\Delta t$; the velocities used to compute the final departure point would be found by interpolation to the position $x_3 - 0.5u_3\Delta t$. If $u_3\Delta t$ is so large that this position is between x_1 and x_2, then a logic problem has arisen: the velocity used to compute the final departure point should be interpolated from u_1 and u_2; that is, u_3 is no longer used directly. Thus, if $0.5u_3\Delta t$ is larger than the distance between grid points, accuracy of the departure point depends on assumptions about the linearity of velocities over distances larger than a grid spacing.

A means of avoiding this potential inaccuracy is to break the large SLT time step Δt down into many small time steps, as discussed in section 2b(1). In the experiments here, the 180-s time step of the underlying model is so small that none of the 180**u** values exceeds the distance between two neighboring grid points. That is, in our one-dimensional example, $x_3 - u_3\Delta t$ is always between x_2 and x_3. Thus one could use a very large number of 180-s time steps to make up one large SLT displacement vector **d**. After each of these small time steps, the departure position would be checked so that when the trajectory leaves the space between x_2 and x_3, interpolation using velocities u_1 and u_2 would be used to compute the continuation of the trajectory. And so on. The total number of 180-s time steps could therefore be as large as desired. However, two considerations arise. First, new logic routines, to check the intermediate departure positions against the grid, must be included in the model. Second, as the number of small time steps gets large, memory requirements of the model simultaneously increase, to retain all the velocities $u_i(t)$ at all times between the beginning and end of the SLT time step.

In the experiments of this paper, the logic problems are eliminated and the memory requirements are held to a reasonable level by limiting the total SLT time step such that no departure point is farther from its arrival point than the distance between two neighboring grid points. This type of limitation is also used by CCM2: the size of all displacement vectors $|\mathbf{d}|$ must always be less than the spacing between adjacent arrival points (Hack et al. 1993).

As noted, the model time step was 3 min for both θ–σ and σ models in all resolutions, and trace constituent transport results were obtained for three values of Δt in (1): 1, 5, and 15 time steps. Nothing larger than 15 (45 min) was used due to the limitation described above; because of the extremely large number of interpolations, particularly for the higher-resolution σ models, only a few experiments with $\Delta t = 1$ time step were undertaken.

3) The interpolations of trace constituent

All interpolations in the experiments here are one-dimensional; the two-dimensional interpolations in the θ–σ models and the three-dimensional interpolations in the σ models are obtained by interpolating first along one model coordinate, and then along the other(s) in sequence. The method for two dimensions using a fourth-order (cubic) interpolation is illustrated in Fig. 1, an adaptation of Fig. 1 of Purser and Leslie (1991). The solid circles are the model grid points **x**, also denoted as (x_i, y_j), at which the values $q(\mathbf{x}, t)$, or q_{ij}, are known; one ''departure point'' $\mathbf{x} - \mathbf{d}$ to which q must be interpolated is the open circle bounded by the constant x_2, x_3, y_2, and y_3 lines. Two-dimensional interpolations were accomplished with four interpolations along constant y_j to the ''$\times$'' points on the dashed line, followed by one interpolation along the dashed line to obtain q at the open circle. Hereafter this is referred to as the ''standard'' interpolation method. Under adiabatic conditions, the four x-direction and one y-direction interpolations, shown in Fig. 1, are sufficient for a fourth-order two-dimensional interpolation in the θ domain of

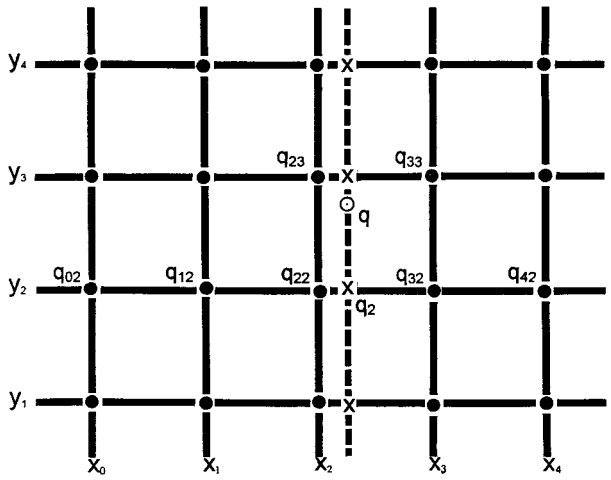

FIG. 1. Schematic of the grid for fourth-order two-dimensional interpolations.

the θ–σ model. In the σ model, a fourth-order three-dimensional interpolation [except the CCM2 emulations described in section 2b(3)] requires 21 individual interpolations: four on each of four model layers in the x direction, followed by four in the y direction, followed by one in the z direction.

In all interpolations, values of q_{ij} are required on both sides of the arrival points. When these adjacent q_{ij} do not exist (i.e., near the north/south walls of the channel, or model top/bottom), equally spaced positions outside the domain were assumed to exist with the same q as at the closest domain grid point.

Interpolation algorithms can be classified as allowing or not allowing over- and undershoots; experiments here included interpolations of both kinds. In Fig. 1, eliminating overshoots would mean that the interpolated q would be adjusted, if necessary, to be no larger than any of q_{22}, q_{23}, q_{32}, and q_{33}. Interpolations that allow undershoots can produce trace constituent less than zero. In the experiments here, all negative values were reset to zero each time step. Conservation of total domain trace constituent was accomplished, regardless of whether the algorithm could create negative q, by computing total constituent TQ at the conclusion of each time interval, and then multiplying every q value by TQ_0/TQ where TQ_0 is total domain constituent in the initial atmosphere, in the same fashion as the ''global fixer'' of Part I.

The interpolations in experiments here, which allow over- and undershoots, are the Lagrangian and an ''overlapping polynomial.'' Lagrangian interpolations use polynomials, which exactly reproduce the known q_{ij} values at a given number of neighboring grid points. For example, the fourth-order accurate cubic Lagrangian may be written as

$$q = a + bx + cx^2 + dx^3. \tag{2}$$

If (2) were applied in Fig. 1 to compute the value q_2, a, b, c, and d would produce exactly the values q_{12} for $x = x_1$, q_{22} for $x = x_2$, q_{32} for $x = x_3$, and q_{42} for $x = x_4$, respectively. The general formula for a Lagrangian interpolation of any order accuracy is provided in many places (e.g., Purser and Leslie 1991). Experiments here include second-, fourth-, sixth-, eight-, tenth-, and twelfth-order Lagrangian interpolants; the sixth through twelfth are used only in conjunction with the ''cascade'' approach of Purser and Leslie (1991), described in section 2b(4).

A second means of choosing the coefficients a, b, c, and d in (2) was also used in experiments here: the ''overlapping polynomial'' technique described by Whittaker and Petersen (1977), where the polynomial was a quadratic. Again referring to Fig. 1, the quadratic $q_1 = a_1 + b_1x + c_1x^2$ was fit to q_{12}, q_{22}, and q_{32} exactly; the quadratic $q_2 = a_2 + b_2x + c_2x^2$ was fit to q_{22}, q_{32}, and q_{42} exactly; and the total interpolant between x_2 and x_3 was

$$q = (1 - \Delta x)q_1 + \Delta x q_2, \tag{3}$$

where $\Delta x = (x - x_2)/(x_3 - x_2)$. This overlapping quadratic (hereafter OQ) interpolant fits the values of q_{22} and q_{32} exactly but not q_{12} or q_{42}. The OQ has the property that the derivative is continuous for a series of interpolants. That is, the derivative $\partial q/\partial x$ at (x_2, y_2) derived from q_{12}, q_{22}, q_{32}, and q_{42} would be equal to the derivative determined from q_{02}, q_{12}, q_{22}, and q_{32}.

Algorithms that eliminate over-and undershoots, employed in experiments here, were the quasi-monotonic approach (hereafter QM) described by Bermejo and Staniforth (1992), the ''shape-preserving'' algorithm of CCM2 as discussed in section 2b(3), and two shape-preserving algorithms described by Holnicki (1995). The QM approach resets, where necessary, the interpolated value of q to be no larger or smaller than the values at the nearest grid points. For example, QM limits the interpolated q in Fig. 1 to the range bounded by the largest and smallest of q_{22}, q_{32}, q_{23}, and q_{33}. In the σ model experiments, comparisons were made to the nearest eight arrival point values: four on the model level below the departure point and four above. As described by Bermejo and Staniforth (1992), QM does not specify the interpolant formula; QM was applied in the experiments here only with Lagrangian fourth-order and the ''cascade'' scheme described in section 2b(4).

Holnicki (1995) describes a class of interpolants, which use the sixth-order polynomial

$$q = a + bx + cx^2 + dx^3 + ex^4 + fx^5. \tag{4}$$

Like the fourth-order Lagrangian, an exact fit is made to four adjacent q_{ij}; the two remaining degrees of freedom in (4) are used to specify the derivatives at the two internal grid points. Holnicki provides four formulas by which the derivatives may be estimated; two of these, the ''harmonic mean'' (hereafter HM) and the ''Akima'' were used here. The HM derivative is given by

$$d_j = \frac{2\Delta_{j-1}\Delta_j}{\Delta_{j-1} + \Delta_j} \tag{5}$$

if the numerator is positive and by zero otherwise. The Akima derivative is given by

$$d_j = \frac{\alpha\Delta_{j-1} + \beta\Delta_j}{\alpha + \beta} \quad \text{if } \alpha + \beta \neq 0, \quad \text{and by}$$

$$d_j = \frac{\Delta_{j-1} + \Delta_j}{2} \qquad \text{otherwise.} \tag{6}$$

In both (5) and (6), $\Delta_j = (q_{j+1} - q_j)/h$ where h is the distance between the j and $j + 1$ positions. In (6), $\alpha = |\Delta_{j+1} + \Delta_j|$ and $\beta = |\Delta_{j-1} + \Delta_{j-2}|$. These derivative estimates are "shape-preserving," which means $q(\mathbf{x} - \mathbf{d}, t)$ is constrained to lie between the values at the neighboring grid points. In the Akima derivatives, the diagram of Fig. 1 is not adequate to illustrate all one-dimensional interpolations required for a complete two-dimensional interpolation to the departure point: six in the x direction followed by one in the y direction. In the σ models, the Akima derivative scheme requires a total of 43 one-dimensional interpolations.

Altogether, experiments were undertaken with a total of 10 trace constituent interpolants, not counting the CCM2 experiments described in section 2b(3): six Lagrangian, the OQ, the HM and Akima derivative estimates of Holnicki, and QM with fourth-order Lagrangian.

4) The CCM2 interpolations

The experiments emulating CCM2 used the shape-preserving interpolation described by Hack et al. (1993) to obtain the interpolated q's. The interpolations, unlike all others in the present experiments, are not genuinely three-dimensional. The SLT interpolations for trace constituents in CCM2 are performed first in the quasi-horizontal model planes, producing intermediate values at the model grid points, followed by vertical interpolations in each model column from these intermediate values. The interpolations to obtain $q(\mathbf{x} - \mathbf{d}, t)$ are fourth-order Lagrangian, the same as the CCM2 interpolations of the velocities, but are modified by a shape-preserving adjustment. Additional experiments were done in which the shape-preserving aspect was turned off; these experiments are designated CCM2 (No P).

The trace constituent interpolations emulating CCM2 in the UW σ model are nearly identical to those in CCM2, the difference being the UW lat–long grid versus the CCM2 Gaussian grid. By virtue of the adiabatic conditions of these experiments, interpolations in the θ–σ models were only in the θ domain, and therefore used only two-dimensional quasi-horizontal interpolations.

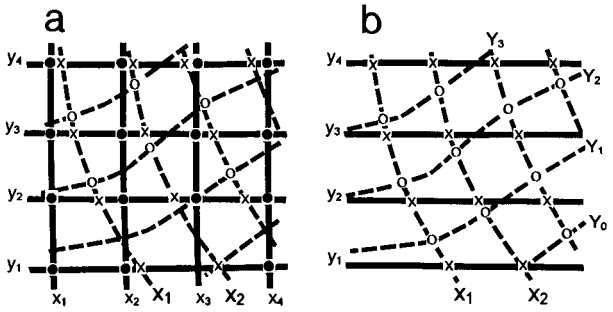

FIG. 2. Development of the cascade grid for two-dimensional interpolations. (a) The ×'s on the grid denote the first interpolation points in the x direction, producing the X_i values on the initial constant y_j axes. (b) The intermediate X_i values are interpolated to the final values at (X_i, Y_j), the open circles.

5) Cascade interpolations

Increasing computational resources are required as the order of accuracy of standard interpolation increases. For example, in three dimensions the standard Lagrangian eighth order requires 73 interpolations for each grid point each time interval. To meet this problem, Purser and Leslie (1991) devised the cascade approach. The idea is illustrated in Fig. 2 (adapted from Fig. 2 of Purser and Leslie) where the SLT arrival points (open circles) are thought of as the grid points (X_i, Y_j) of a completely new coordinate system, shown as the dashed lines in Figs. 2a and 2b. In two dimensions, the first cascade computations are of the positions marked as x in Fig. 2a at which the constant X_i coordinates cross the constant y_j coordinates. These positions, the grid points of an intermediate grid, are found from the x-coordinate velocities at (x_i, y_j). Values of q are then interpolated to these (X_i, y_j) positions. Next, the Y_j positions along the dashed X_i coordinate lines are determined using y-coordinate velocities. Finally values of q at (X_i, Y_j) are interpolated from the intermediate values at the (X_i, y_j) positions. Three-dimensional interpolations for the σ models require an additional set of intermediate coordinates and of interpolated q values.

The critical point about the cascade technique is that only two or three interpolations (for two- or three-dimensions, respectively) of transported constituent are required per grid point, a sharp reduction from the standard approach. The reduction is accomplished by computing values for the entire intermediate grid before any interpolations are undertaken in the following coordinate direction(s). The reduction of trace constituent interpolations is somewhat offset by an increase in the number of computations required to find the intermediate grid points. The results of timing tests for the $\sigma(43)$ model on a scalar computer are shown in Table 1, in which the time required for the underlying model (i.e., without any transport or advection of trace constituent) is subtracted off and the remaining time for the standard Lagrangian fourth-order trace constituent interpolant is set to unity as the reference. As seen in

TABLE 1. Run time ratios for SLT interpolants relative to the standard Lagrangian fourth order, for the $\sigma(43)$ model.

	Standard	Cascade
Lagrangian 2d order	0.49	0.65
Lagrangian 4th order	1.00	0.74
Lagrangian 6th order	3.0*	0.90
Lagrangian 8th order	4.4*	0.96
Lagrangian 10th order	—	1.06
Lagrangian 12th order	—	1.21
OQ	1.22	0.79
QM	1.03*	0.77
HM	3.3	1.17*
Akima	20	1.60*
CCM2	1.07	—

* Only timing tests were undertaken for these models.

Table 1, the total time for even the Lagrangian 10th-order interpolant with cascade is only slightly more than the standard fourth order. (Table 1 shows that for the Lagrangian second order, the cascade scheme is slower than the standard. This result is of purely academic interest since the Lagrangian second-order interpolant is inadequate for predictions, as shown in section 3d. Nonetheless, it shows that the time required to compute the cascade grid, termed ''overhead'' by Purser and Leslie, is not negligible.) The remaining obvious question, whether cascade interpolation produces the same results as the standard, is addressed in section 3a.

3. Results

As discussed in the introduction, under the adiabatic conditions of these simulations the maximum value of inert trace constituent and the areas between any two trace constituent contour values should remain constant on all explicit or implicit isentropic surfaces. The primary means of comparing results between the various SLT algorithms, time intervals, model types, and model resolutions is to examine these quantities on the 310 K isentropic layer. The data in Tables 2, 3, and 4 are ratios of constituent maxima on 310 K at the end of 48-h integrations to the maximum in the initial atmosphere; ideally all values in these tables would be unity.

An extremely large number of experiments were performed: two-resolution θ–σ and four-resolution σ models; one-step and multiple-step displacement vector computations for two different time intervals and sometimes three (when interpolations every time step did not require too much computer time); 10 different interpolants, with three in both the standard and cascade interpolation grids; two additional experiments emulating CCM2; and two initial trace constituent distributions. In examining the various combinations of these options, the results for θ–$\sigma(3.33)$ and θ–$\sigma(5)$ were essentially the same; and the results for the σ models typically show the same progression and improvement from the lowest resolution $\sigma(19)$ to the highest resolution $\sigma(43)$ model as found in the advection experiments of Part I. Consequently, only a portion of the overall data need be presented to provide a full review of the experiments.

a. Cascade versus standard interpolations

Table 2 shows the cascade trace constituent maxima on 310 K compared to the standard interpolations, for the θ–$\sigma(3.33)$ and $\sigma(43)$ models. The comparison is made for three interpolants: the second- and fourth-order Lagrangian and OQ. Results are shown only for the one-step computation of displacement vectors and the 15 time step time interval. As seen, the standard and cascade results are quite similar. The maximum difference for both models and all resolutions is less than 0.5%. Since the reduction in computer time achieved by the cascade approach is dramatic, as shown in Table 1 and also as reported by Purser and Leslie (1991), these experiments made possible the cascade tests with Lagrangian interpolants of sixth order and higher.

b. One-step versus multiple-step displacement vectors

For the θ–σ models, very little difference occurred in either the maxima on 310 K or in the distributions for the one-step computations of displacement vectors compared to multiple step, in either vertical resolution for any of the trace constituent interpolants of q. The largest difference (not shown) between maxima on 310 K for the five–time step interval was 0.2% and for the 15 time step interval was 0.4%. Of the other 38 individual cases, the largest difference for 31 was no more than 0.1%.

TABLE 2. Comparison of cascade and standard interpolation procedures for the θ–$\sigma(3.33)$ and $\sigma(43)$ models. Values shown are Q_{max}(48-h)/Q_{max}(0-h) where Q_{max} is on 310 K, for one-step displacement vector and 15 time-step interval.

		310K		660P	
		Standard	Cascade	Standard	Cascade
Lagrangian 2d	θ–$\sigma(3.33)$	0.737	0.737	0.589	0.588
	$\sigma(43)$	0.617	0.619	0.463	0.461
Lagrangian 4th	θ–$\sigma(3.33)$	1.003	1.004	0.897	0.899
	$\sigma(43)$	0.891	0.890	0.781	0.779
OQ	θ–$\sigma(3.33)$	1.105	1.105	0.965	0.969
	$\sigma(43)$	0.941	0.939	0.818	0.816

TABLE 3. Effect of time interval (1, 5, or 15 time steps) for three interpolants: Q_{max}(48-h)/Q_{max}(0-h) on 310 K for the θ–σ(3.33) and σ(43) models for both distributions.

Time interval (time steps)		310K			660P		
		1	5	15	1	5	15
OQ	θ–σ(3.33)	1.180	1.158	1.104	1.044	1.020	0.964
	σ(43)	1.009	1.010	0.964	0.834	0.837	0.838
HM derivative	θ–σ(3.33)	0.922	0.940	0.927	0.809	0.871	0.872
	σ(43)	—*	0.821	0.804	—*	0.813	0.780
Akima derivative	θ–σ(3.33)	0.928	0.951	0.961	0.843	0.900	0.909
	σ(43)	—*	0.829	0.893	—*	0.817	0.815

* Simulation not performed due to extreme computer requirements.

For the σ models, the differences between the one-step and multiple-step maxima on the 310 K level are also small, though not as small as for the θ–σ(3.33) model. The differences were less than 0.2% for the HM and Akima derivative estimates, while differences were less than 1% for the Lagrangian second order. For the other interpolants, differences were sometimes as large as 3%. However, in no experiment were the one-step maxima consistently larger or smaller than those for the multiple step.

Only small differences occur between the multiple-step displacement vector computations, which use the velocity data for all time steps, and the one-step computations, which use the velocities before the first and after the last time step during each SLT time interval. The critical point (following CCM2; Hack et al. 1993) is that the departure points be no further from the arrival points than one grid spacing; a more stringent limitation seems unnecessary. Because of the small differences, none are presented in tabular form.

c. *Effect of the SLT time interval*

As discussed in section 2b, the SLT time intervals were restricted to 1, 5, and 15 time steps. Because of computational requirements, neither the HM or Akima derivatives were attempted for the 1 time step case for the σ models. Timing results are shown in Table 1.

For both the θ–σ and σ models, the results of maximum trace constituent on 310 K for the Lagrangian interpolants, for all orders fourth through twelth, are virtually unaffected by the different time interval choices; differences are less than 1% (not shown). The second-order Lagrangian (known to be inaccurate) shows differences as large as 4%. In addition, the maxima on 310 K for the 5 and 15 time step time intervals tested for CCM2 show only small differences; and differences between all three time intervals are small for the QM case. It is not surprising that the CCM2 and QM results are similar to the Lagrangian since both are essentially fourth-order Lagrangian interpolants with changes to prevent over- and undershoots.

TABLE 4. Ratio of Q_{max}(48-h)/Q_{max}(0-h) on the 310 K surface for all interpolants and both distributions. All SLT data are for 15 time step time intervals and one-step displacement vector computations.

Model	310K			660P		
	θ–σ(3.33)	σ(27)	σ(43)	θ–σ(3.33)	σ(27)	σ(43)
Lagrangian 2d[a]	0.737	0.606	0.619	0.736	0.402	0.588
Lagrangian 4th[a]	1.003	0.835	0.891	0.897	0.716	0.781
Lagrangian 6th[a]	1.027	0.928	0.971	0.968	0.816	0.875
Lagrangian 8th[a]	1.038	0.958	0.985	0.991	0.856	0.912
Lagrangian 10th[a]	1.040	0.971	0.987	0.998	0.877	0.933
Lagrangian 12th[a]	1.040	0.976	0.987	0.999	0.890	0.947
OQ[a]	1.105	0.961	0.941	0.965	0.796	0.818
QM[a]	0.967	0.828	0.876	0.895	0.705	0.778
HM	0.927	0.802	0.804	0.872	0.776	0.780
Akima	0.963	0.862	0.883	0.911	0.808	0.821
CCM2	0.911	0.760	0.811	0.805	0.648	0.724
CCM2 (No P)	1.002	0.866	0.932	0.897	0.739	0.811
Part I results[b]						
Standard	1.115	1.104	1.093	0.997	0.976	0.902
Simple upstream	0.696	0.589	0.604	0.547	0.376	0.421
PPM	0.984	0.810	0.934	0.885	0.896	0.945
CSOM	1.037	0.896	0.945	1.049	0.905	0.950

[a] Results using the cascade multidimensional technique.

[b] Standard is second-order finite differencing; PPM is piecewise parabolic method, following Carpenter et al. (1990); CSOM is conservation of second-order moments, following Prather (1986).

Fairly significant differences occur for the other three interpolants, the HM and Akima derivative estimates, and the OQ. Results for the θ–σ(3.33) and σ(43) models, shown in Table 3, depict differences for the different time intervals as large as 8%. The explanation for these inconsistencies seems to be that these three interpolants are subject to larger numerical noise than the Lagrangian. The five time step interval requires three times as many interpolations as the 15 time step intervals, providing more opportunities for numerical noise to have an effect. An alternative explanation might be based on the fact that the distances |**d**| are larger for larger time intervals so that interpolations are made to positions further from the known values; however, in light of section 3b the distances |**d**| seem to be reasonable.

d. Effects of the interpolants

A basic reason for these experiments was to develop an understanding of which trace constituent interpolant is best in SLT. Of course, many interpolants are not examined here, such as spline functions or variations of the ones tested here (such as QM with a higher-order Lagrangian). Nevertheless, the experiments provide several clear preferences. Conservation of maxima results for all the interpolants tested are presented in Table 4 for the σ(27), σ(43), and θ–σ(3.33) models.

The first result of interest is found in a comparison of the various Lagrangian interpolants. As seen, the second-order provides relatively poor conservation results for both distributions and both models: the maxima on 310 K are substantially smaller than the ideal of unity, with some as low as 0.4. As the order of Lagrangian interpolation increases, the maxima increase monotonically, for all three models and both initial distributions. Net overshoots occur for the θ–σ(3.33) model for the 310K distribution, with maxima a few percent higher than unity for the fourth- and higher-order accuracies, but not for the 660P distribution or any of the σ models. Taken together, these results show that improvements in accuracy of conservation (nearness to unity) are small for orders greater than eighth.

A comparison of the σ(27) and σ(43) model data for all the interpolants in Table 4 is instructive. Other than one exception, the OQ interpolant for the 310K distribution, every trace constituent maximum for the σ (27) model is less than the corresponding value for the σ (43) model. Also for the 310K distribution, the σ(27) trace maximum value is less than 0.90 for every interpolant except the Lagrangian sixth through twelfth order. These results suggest that high vertical resolution is important for accuracy in σ models employing SLT, regardless of the interpolant.

Three of the interpolants are shape-preserving: the HM and Akima derivatives and the CCM2 emulation. The two CCM2 emulations are particularly instructive: similar to the results of Zapotocny et al. (1997), the CCM2 (No P) case produces results significantly closer to the ideal of unity, for all three models and both distributions. The HM derivative is consistently less accurate than the Akima derivative; and this latter interpolant produces trace constituent maxima, which are significantly less accurate than the Lagrangian sixth order. Finally, the QM (the Lagrangian fourth-order interpolant with a ''fixer'' to prevent over- and undershoots) produces results that are somewhat less accurate than the corresponding Lagrangian fourth-order results. These results taken together suggest that shape preservation and enforced monotonicity cause reduced accuracy with respect to conserving trace constituent maxima.

A comparison of trace constituent maxima in Table 4 between the two distributions shows that every value for the 310K distribution is larger than the corresponding value for the 660P distribution. A comparable result was found for the various methods of transporting trace constituent in Part I, where it was noted that the 660P distribution is narrower north to south than the 310K. This result suggests that sharper distributions are subject in SLT, as in advection, to greater numerical diffusion even for extremely high order Lagrangian interpolants.

Every trace constituent maximum on 310 K in Table 4 is larger for the θ–σ model than the corresponding value for either the σ(27) or σ(43) model. For the 310K distribution, the θ–σ model produces overshoots for the fourth- through twelfth-order Lagrangian interpolants, which produces values somewhat further from unity than values for the σ(43) model for the eighth- through twelfth-order Lagrangian. Other than these cases, the θ–σ(3.33) produces trace constituent maxima more accurately than either σ model, for all interpolants and both initial distributions.

A comparison between the Lagrangian interpolants and CCM2 (No P) is revealing. For the θ–σ models, the only difference between the CCM2 (No P) and Lagrangian fourth-order is the means of interpolating velocities: since the experiments are under adiabatic conditions, only two-dimensional trace constituent interpolations are required. The Lagrangian fourth-order SLT experiments here use linear interpolation of velocities whereas CCM2 (No P) uses fourth-order Lagrangian. As shown in Table 4, θ–σ model results for the fourth-order Lagrangian SLT and CCM2 (No P) trace constituent maxima on 310 K are virtually identical, for both initial distributions. For the σ models, however, in addition to velocities, CCM2 (No P) first does a two-dimensional trace constituent interpolation on model levels followed by a one-dimensional vertical interpolation at the grid columns, whereas the Lagrangian SLTs (regardless of order) do all three dimensions the same way. Interestingly, the CCM2 (No P) simulations produce a higher degree of conservation of trace constituent on 310 K than the fourth-order Lagrangian, for both distributions and all four vertical resolution σ models [results for σ(19) and σ(35) are not shown]. However,

TABLE 5. Conservation of areas between contours: Ratios of 48-h predictions to values in the initial distributions, for 15 time step time intervals and one-step displacement vector simulations.

	310K initial distribution				660P initial distribution			
Scheme/bin	0–1	1–4	4–7	7–max	0–1	1–4	4–7	7–max
Lagrangian 2d cascade								
θ–σ(5)	0.870	1.250	1.845	0.087	0.911	1.632	1.571	0.000
θ–σ(3)	0.871	1.250	1.836	0.087	0.965	1.151	1.122	1.219
σ(19)	0.953	1.647	0.302	0.000	0.908	2.150	0.000	0.000
σ(27)	0.936	1.616	0.582	0.000	0.908	2.195	0.000	0.000
σ(35)	0.938	1.521	0.734	0.000	0.908	2.139	0.118	0.000
σ(43)	0.933	1.461	0.929	0.000	0.909	2.101	0.255	0.000
Lagrangian 4th cascade								
θ–σ(5)	0.955	1.043	1.121	1.145	0.962	1.132	1.347	1.063
θ–σ(3)	0.957	1.036	1.121	1.159	0.961	1.151	1.327	1.063
σ(19)	0.969	1.132	1.267	0.268	0.942	1.425	1.382	0.000
σ(27)	0.956	1.111	1.282	0.632	0.949	1.322	1.673	0.000
σ(35)	0.969	1.060	1.211	0.783	0.956	1.245	1.706	0.129
σ(43)	0.969	1.056	1.196	0.812	0.958	1.221	1.686	0.226
Lagrangian 6th cascade								
θ–σ(5)	0.959	1.025	1.121	1.174	0.962	1.151	1.204	1.188
θ–σ(3)	0.962	1.025	1.112	1.159	0.965	1.125	1.204	1.219
σ(19)	0.967	1.096	1.112	0.786	0.949	1.340	1.382	0.231
σ(27)	0.954	1.107	1.173	0.853	0.958	1.255	1.500	0.333
σ(35)	0.967	1.056	1.156	0.913	0.961	1.219	1.510	0.419
σ(43)	0.965	1.070	1.125	0.913	0.962	1.201	1.549	0.419
Lagrangian 8th cascade								
θ–σ(5)	0.960	1.025	1.112	1.174	0.963	1.171	1.122	1.188
θ–σ(3)	0.962	1.021	1.112	1.174	0.965	1.151	1.122	1.219
σ(19)	0.964	1.088	1.103	0.893	0.952	1.320	1.364	0.269
σ(27)	0.955	1.107	1.164	0.853	0.960	1.228	1.462	0.467
σ(35)	0.965	1.056	1.174	0.899	0.964	1.199	1.373	0.613
σ(43)	0.965	1.067	1.134	0.913	0.965	1.188	1.392	0.613
Lagrangian 10th cascade								
θ–σ(5)	0.959	1.032	1.121	1.145	0.968	1.138	1.082	1.250
θ–σ(3)	0.959	1.032	1.112	1.159	0.965	1.151	1.122	1.219
σ(19)	0.964	1.085	1.112	0.893	0.955	1.294	1.364	0.308
σ(27)	0.956	1.103	1.164	0.853	0.962	1.228	1.346	0.567
σ(35)	0.968	1.042	1.202	0.884	0.964	1.205	1.294	0.710
σ(43)	0.969	1.046	1.161	0.913	0.963	1.215	1.314	0.677
Lagrangian 12th cascade								
θ–σ(5)	0.962	1.032	1.103	1.145	0.969	1.118	1.122	1.250
θ–σ(3)	0.959	1.036	1.103	1.159	0.963	1.132	1.327	1.063
σ(19)	0.964	1.081	1.112	0.911	0.955	1.288	1.345	0.385
σ(27)	0.960	1.092	1.164	0.853	0.965	1.208	1.346	0.567
σ(35)	0.969	1.035	1.202	0.899	0.968	1.185	1.275	0.710
σ(43)	0.969	1.042	1.170	0.913	0.967	1.195	1.275	0.710
CCM2								
θ–σ(5)	0.949	1.043	1.207	1.072	0.961	1.138	1.571	0.750
θ–σ(3)	0.949	1.046	1.207	1.058	0.960	1.151	1.571	0.719
σ(19)	0.961	1.158	1.371	0.036	0.936	1.510	1.255	0.000
σ(27)	0.943	1.155	1.527	0.221	0.944	1.349	1.692	0.000
σ(35)	0.953	1.095	1.413	0.507	0.949	1.258	1.882	0.000
σ(43)	0.957	1.088	1.313	0.638	0.951	1.255	1.863	0.000
CCM2 (No P)								
θ–σ(5)	0.957	1.036	1.112	1.174	0.962	1.138	1.367	1.000
θ–σ(3)	0.958	1.029	1.129	1.159	0.963	1.132	1.306	1.094
σ(19)	0.966	1.121	1.310	0.268	0.940	1.418	1.436	0.000
σ(27)	0.950	1.111	1.264	0.735	0.949	1.275	1.769	0.067
σ(35)	0.962	1.046	1.266	0.841	0.954	1.225	1.725	0.258
σ(43)	0.962	1.053	1.214	0.884	0.955	1.208	1.725	0.323

TABLE 5. (*Continued*).

	310K initial distribution				660P initial distribution			
Scheme/bin	0–1	1–4	4–7	7–max	0–1	1–4	4–7	7–max
OQ cascade								
θ–σ(5)	0.960	1.054	1.121	1.043	0.966	1.118	1.408	0.906
θ–σ(3)	0.964	1.036	1.129	1.058	0.965	1.105	1.469	0.906
σ(19)	0.959	1.092	1.181	0.786	0.953	1.301	1.491	0.077
σ(27)	0.950	1.107	1.218	0.824	0.957	1.201	1.692	0.300
σ(35)	0.967	1.053	1.193	0.870	0.962	1.152	1.725	0.323
σ(43)	0.968	1.049	1.196	0.855	0.962	1.168	1.627	0.419
QM								
θ–σ(5)	0.955	1.039	1.147	1.116	0.962	1.132	1.347	1.063
θ–σ(3)	0.954	1.043	1.138	1.130	0.961	1.145	1.347	1.063
σ(19)	0.969	1.132	1.284	0.232	0.942	1.438	1.345	0.000
σ(27)	0.956	1.111	1.291	0.618	0.949	1.329	1.654	0.000
σ(35)	0.968	1.063	1.220	0.768	0.954	1.258	1.725	0.097
σ(43)	0.969	1.060	1.188	0.812	0.956	1.235	1.686	0.226
Akima								
θ–σ(5)	0.960	1.057	1.086	1.087	0.959	1.178	1.327	1.000
θ–σ(3)	0.958	1.061	1.078	1.116	0.959	1.171	1.367	0.969
σ(19)	0.966	1.154	1.052	0.643	0.960	1.288	1.109	0.654
σ(27)	0.956	1.155	1.064	0.809	0.961	1.228	1.404	0.533
σ(35)	0.965	1.099	1.092	0.855	0.961	1,245	1.392	0.484
σ(43)	0.968	1.099	1.045	0.899	0.965	1.201	1.451	0.452
HM								
θ–σ(5)	0.955	1.075	1.060	1.116	0.958	1.158	1.347	1.094
θ–σ(3)	0.955	1.071	1.078	1.101	0.958	1.171	1.286	1.125
σ(19)	0.955	1.169	1.155	0.518	0.952	1.386	1.236	0.154
σ(27)	0.949	1.170	1.173	0.662	0.959	1.228	1.538	0.367
σ(35)	0.967	1.109	1.138	0.725	0.964	1.199	1.490	0.419
σ(43)	0.968	1.106	1.116	0.754	0.966	1.215	1.471	0.323

the Lagrangian sixth order produces better results than the CCM2 (No P) case.

e. Conservation of areas between trace constituent contours

As in Part I, trial and error led to the conclusion that the contour intervals 0–1, 1–4, 4–7, and 7–max units of trace constituent (where the initial atmosphere has a maximum of 10 units) provide reasonable information for review. Data for one step and 15Δt time step displacement vector simulations are found in Table 5, where the numbers of grid points in each bin were normalized against the value in the initial atmosphere, producing bias values. A simulation producing values of exactly one in each bin would represent a perfect bias. Data for the other SLT time step choices (1Δt and 5Δt, and multiple step) do not show significant differences.

In the experiments utilizing various Lagrangian cascade algorithms, a natural progression of improving bias values may be seen from second to twelfth order. However, for both initial distributions, little practical improvement is realized in tenth or twelfth orders. A second conclusion from Table 5, similar to the conservation of initial maxima in Table 4, is that the 310K initial distribution achieves substantially better bias scores than the 660P distribution. A third conclusion, similar to that reached from examination of Table 4, is that the interpolations of CCM2 have better bias values when shape preservation is not invoked. Fourth, the interpolations of CCM2 are worse than the Lagrangian fourth-order when shape preservation is utilized and better when not used. Finally, of the remaining four algorithms, the Holnicki Akima is best for both distributions, followed by the Holnicki harmonic mean, with the OQ and the QM substantially worse.

f. Comparisons of SLT and advection algorithms

A number of similarities exist between the advection results of Part I and the SLT results reported here. Figures 3 and 4 show 48-h distributions on 310 K for the θ–σ(3.33) and σ(43) models, respectively. Panels a, c, and e in both figures show results for the ''simple upstream'' algorithm, piecewise parabolic method (PPM) following Carpenter et al. (1990) and the conservation of second-order moments (CSOM) following Prather (1986), while panels b, d, and f show the SLT results for the second-, fourth-, and sixth-order order Lagrangian interpolants. As seen, there is a high degree of similarity between the simple upstream advection and Lagrangian second order; between the PPM and Lagrangian fourth order; and between the CSOM and Lagrangian sixth order. (As in Part I, the distributions in Figs.

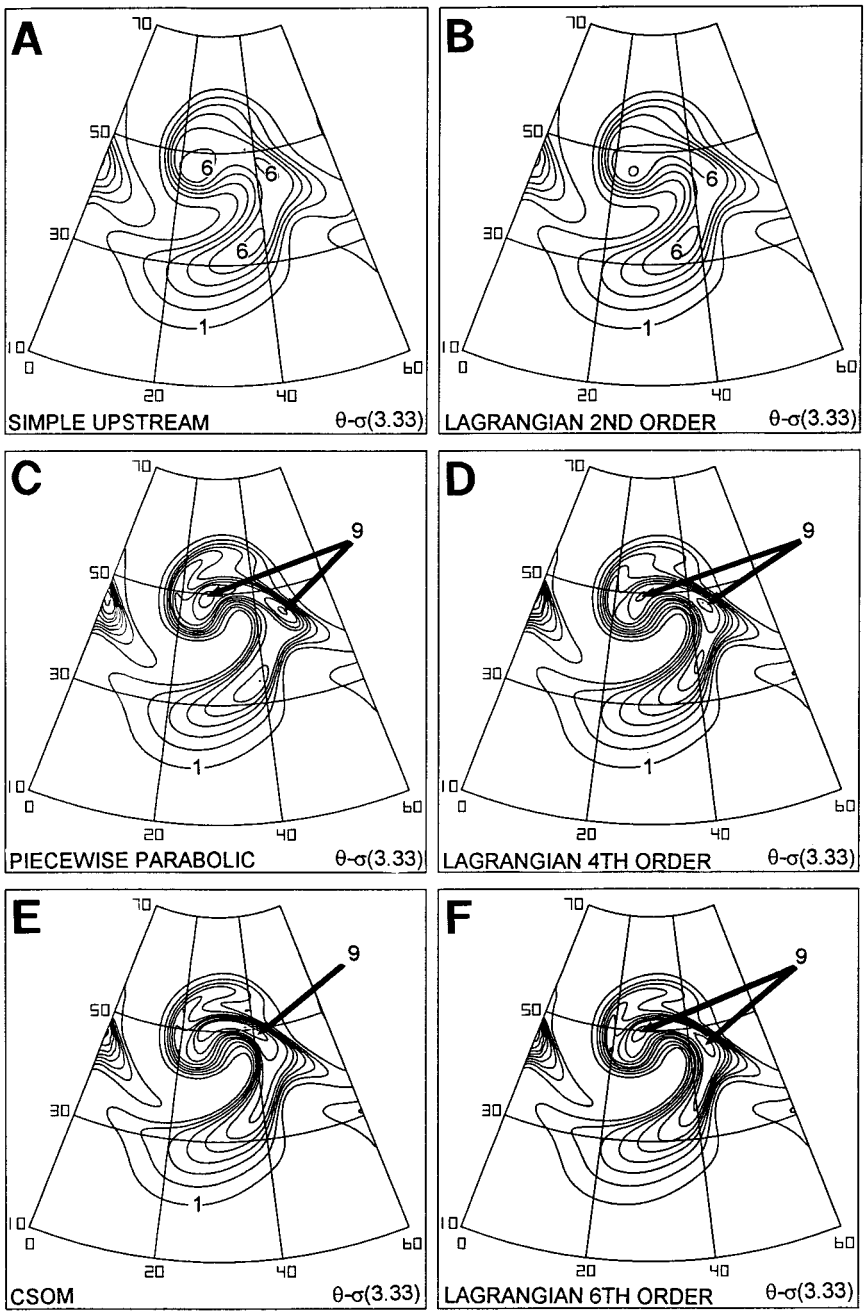

FIG. 3. The 48-h distributions of inert trace constituent on 310 K for the θ–σ(3.33) model, for the 310K initial distribution. The advection scheme or SLT interpolant is noted on the individual panels.

3 and 4 include a 15° wrap from 45° to 60°, for easier visualization.) Table 4 includes four rows of data from Part I giving the values of trace constituent maxima on 310 K for these advection algorithms; similarities are found there also.

In the investigations of Part I, the CSOM algorithm produced the highest degree of consistency in conservation of trace constituent maxima: for each model, the maximum for the 310K distribution was essentially the same as for the 660P. This consistency (shown in Table 4, which includes values from Part I) is not approached by any of the SLT methodologies lower than Lagrangian tenth order. Further, as noted in Part I, the 660P distribution is narrower in the north–south direction than the 310K. Decreased accuracy of conservation for the 660P, for all transport algorithms other than the CSOM, is probably the result of greater numerical diffusion. It is interesting that the SLT calculations, in which the failure

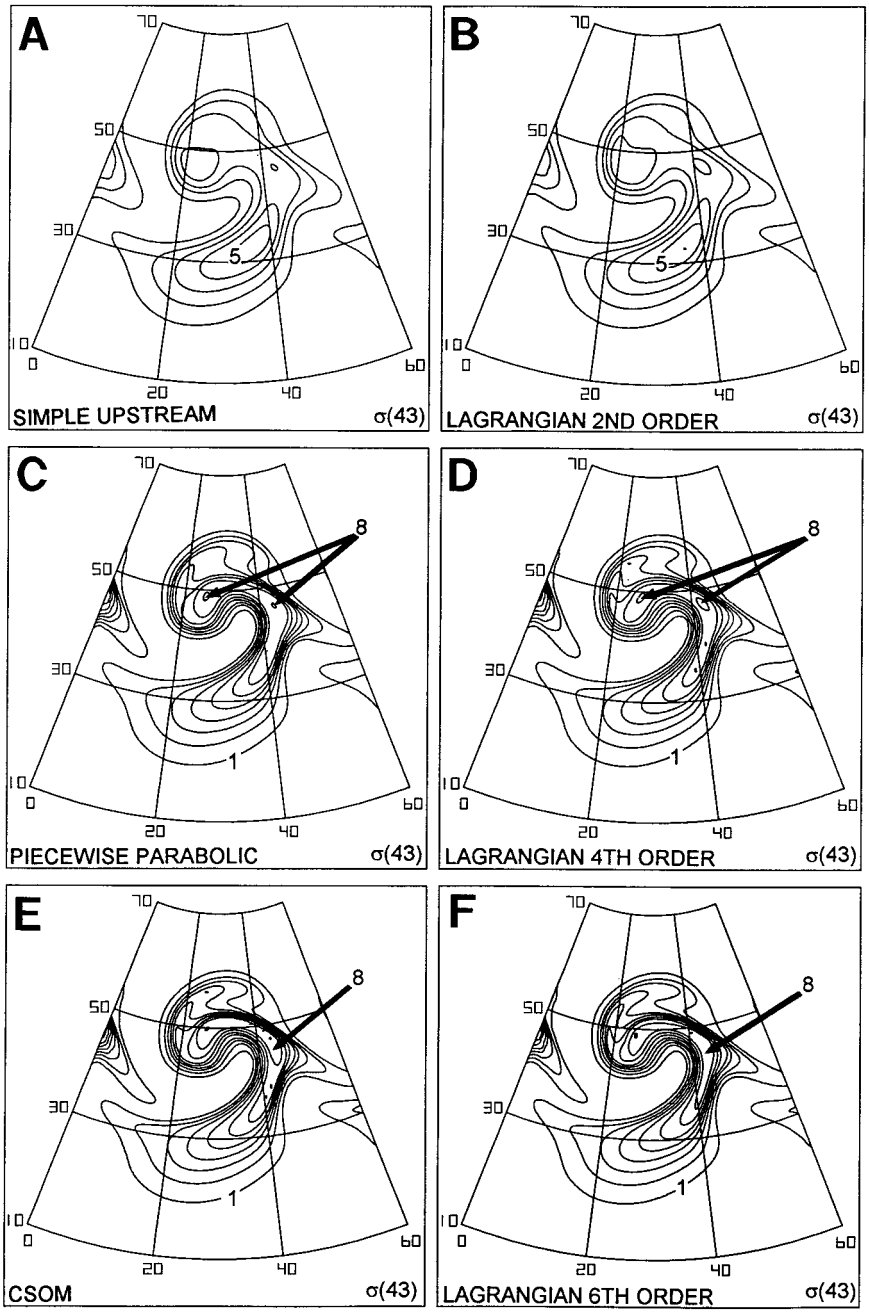

FIG. 4. Same as Fig. 3 except for the $\sigma(43)$ model.

to conserve is probably caused by the inherent smoothing of polynomial interpolants, produce similar results.

For comparison, the CSOM requires approximately one-third the computation time of the sixth-order Lagrangian with the cascade scheme. However, the CSOM must be applied every time step whereas SLT need meet only the $|\mathbf{d}|$ requirement (section 2b), which can be many time steps per time interval; thus the total time required by CSOM, for a comparable time interval, could be larger.

4. Discussion

These three-dimensional 48-h simulations of inert trace constituent transport under adiabatic conditions within an amplifying baroclinic wave provide a means of comparing 10 different SLT interpolants and two emulations of the SLT approach in CCM2. Experiments were done with two vertical resolutions of the UW θ–σ channel model and four vertical resolutions of the UW σ model. An objective measure of accuracy is the

models' ability to conserve the initial maximum value of trace constituent on the 310-K surface. Unlike the more typical one- and two-dimensional tests, these experiments examined a large number of SLT algorithms in an atmosphere with the added complexity of vertical transport. Important results from these experiments are the following.

1) The cascade interpolation approach of Purser and Leslie (1991) is an acceptable means of greatly reducing the computation time involved in the use of higher-order interpolants.
2) Some interpolants appear to produce more numerical noise than others. In these experiments, the HM and Akima derivative estimates of Holnicki (1995) and the OQ algorithm seem to produce larger oscillations by resolution and initial distribution than the Lagrangian interpolants of fourth order or higher.
3) Shape preservation and the QM approach produced less accurate conservation of trace constituent.
4) Lagrangian interpolants of orders second through eighth steadily improve conservation whereas interpolants higher than eighth order do not significantly improve results. This conclusion arises from consideration of both trace constituent maxima and bias scores on contour areas.
5) Accuracy of the θ–σ model in conserving the initial trace constituent maximum is regularly better than the σ model. The 32 θ–σ(3.33) maxima presented in Table 4 were better than 54 of the 64 corresponding σ model results. This is consistent with Zapotocny et al. (1997), who examined conservation characteristics between the global UW θ–σ model and CCM2 using assimilated data as the initial atmosphere. (The 10-day integrations presented in Zapotocny et al. are much more dramatic than the 2-day results here.)

Finally, the results of these experiments re-emphasize two points noted in Part I. First, three-dimensional tests, preferably within a baroclinic wave with substantial vertical motion, are essential for comparing transport or advection algorithms. For example, Holnicki (1995) describes one- and two-dimensional SLT experiments, which suggest that the HM and Akima derivative estimates in sixth-order polynomial interpolants are highly accurate. But in the tests here, both are significantly less accurate than the simpler (both conceptually and calculationally) Lagrangian sixth order. Second, the CSOM advection algorithm (see Part I) of Prather (1986) appears worthy of wider experimentation, due to its combination of consistent high accuracy and apparent low numerical diffusion.

Acknowledgments. Support of the Department of Energy under Grant DE-FG02-92ER61439 and of NASA under Grants NAG5-1330 and NAG5-4398 is gratefully acknowledged. Thanks are due to Prof. Donald R. Johnson for his assistance in both this and Part I, to Dr. Allen J. Lenzen for conversations on SLT in general and how it is used in the CCM2, to Judy Mohr for technical typing assistance, and to Krista Ommodt for graphics support (and for not complaining about the many requests for revisions).

REFERENCES

Bermejo, R., and A. Staniforth, 1992: The conversion of semi-Lagrangian schemes to quasi-monotonic schemes. *Mon. Wea. Rev.*, **120,** 2622–2632.

Carpenter, R. L., Jr., K. K. Droegemeier, P. R. Woodward, and C. E. Hane, 1990: Application of the Piecewise Parabolic Method (PPM) to meteorological modeling. *Mon. Wea. Rev.*, **118,** 586–612.

Hack, J. J., B. A. Boville, B. P. Briegleb, J. T. Kiehl, P. J. Rasch, and D. L. Williamson, 1993: Description of the NCAR Community Climate Model (CCM2). NCAR Tech. Note NCAR/TN-382+STR, 108 pp. [Available from NCAR, P.O. Box 3000, Boulder, CO 80307.]

Holnicki, P., 1995: A shape-preserving interpolation: Applications to semi-Lagrangian advection. *Mon. Wea. Rev.*, **123,** 862–870.

Johnson, D. R., T. H. Zapotocny, F. M. Reames, B. J. Wolf, and R. B. Pierce, 1993: A comparison of simulated precipitation by hybrid isentropic–sigma and sigma models. *Mon. Wea. Rev.*, **121,** 2088–2114.

Junker, N. W., and J. E. Hoke, 1990: An examination of nested grid model precipitation forecasts in the presence of moderate-to-strong low-level southerly inflow. *Wea. Forecasting,* **5,** 333–344.

Kalnay, E., M. Kanamitsu, and W. E. Baker, 1990: Global numerical weather prediction at the National Meteorological Center. *Bull. Amer. Meteor. Soc.,* **71,** 1410–1428.

Kurihara, V., and J. L. Holloway, 1967: Numerical integration of a nine level global primitive equation model formulated by the box method. *Mon. Wea. Rev.*, **95,** 509–529.

Matsuno, T., 1966: Numerical integrations of the primitive equations by a simulated backward difference method. *J. Meteor. Soc. Japan,* **44,** 76–84.

Pierce, R. B., D. R. Johnson, F. M. Reames, T. H. Zapotocny, and B. J. Wolf, 1991: Numerical investigations with a hybrid isentropic–sigma model. Part I: Normal-mode characteristics. *J. Atmos. Sci.,* **48,** 2005–2024.

Prather, M. J., 1986: Numerical advection by conservation of second-order moments. *J. Geophys. Res.*, **91,** 6671–6681.

Purser, R. J., and L. M. Leslie, 1991: An efficient interpolation procedure for high-order three-dimensional semi-Lagrangian models. *Mon. Wea. Rev.,* **119,** 2492–2498.

Reames, F. M., and T. H. Zapotocny, 1999: Inert trace constituent transport in sigma and hybrid isentropic–sigma models: Part I: Nine advection algorithms. *Mon. Wea. Rev.,* **127,** 173–187.

Whittaker, T. M., and R. A. Petersen, 1977: Objective cross-sectional analyses incorporating thermal enhancement of observed winds. *Mon. Wea. Rev.,* **105,** 147–153.

Williamson, D. L., 1990: Semi-Lagrangian transport in the NMC spectral model. *Tellus,* **42A,** 412–428.

Zapotocny, T. H., A. J. Lenzen, D. R. Johnson, T. K. Schaack, and F. M. Reames, 1997: A comparison of inert trace constituent transport between the University of Wisconsin isentropic–sigma model and the NCAR Community Climate Model. *Mon. Wea. Rev.,* **125,** 120–142.